separations

Article

Unlocking the Treasure Box: The Role of HEPES Buffer in Disassembling an Uncommon Ferritin Nanoparticle

Alessio Incocciati [1], Lucia Bertuccini [2], Alberto Boffi [1,3], Alberto Macone [1,*,†] and Alessandra Bonamore [1,*,†]

[1] Department of Biochemical Sciences "Alessandro Rossi Fanelli", Sapienza University of Rome, Piazzale Aldo Moro 5, 00185 Rome, Italy
[2] Core Facilities, Istituto Superiore di Sanità, 00169 Rome, Italy
[3] Center for Life Nano Science@Sapienza, Istituto Italiano di Tecnologia, Viale Regina Elena 291, 00161 Rome, Italy
* Correspondence: alberto.macone@uniroma1.it (A.M.); alessandra.bonamore@uniroma1.it (A.B.)
† These authors contributed equally to this work.

Abstract: Ferritins are ideal nanoparticles as drug delivery systems due to their hollow-sphere structure and the ability to target specific receptors on the cell surface. Here, we develop and characterize a new ferritin derived from the chimeric humanized *A. fulgidus* one, already designed to recognize the TfR1 receptor. Starting from the synthetic gene of this chimeric protein, we replaced two positively charged amino acids with two alanine residues to close the large triangular pores on its surface. These mutations make the protein nanoparticle suitable to incorporate even small therapeutics without leakage. Size-exclusion chromatography shows that the assembling/disassembling of this new protein cage can be easily fine-tuned by varying the HEPES buffer and $MgCl_2$ concentration. The protein cage can be opened using 150 mM HEPES buffer without magnesium ions. Adding this divalent cation to the solution promotes the quick assembly of the ferritin as a 24-mer. The development of this new protein cage paves the way for encapsulation and delivery studies of small molecules for therapeutic and diagnostic purposes.

Keywords: ferritin; self-assembling; HEPES buffer; chromatography; gel filtration; TEM; nanoparticles; mutagenesis

Citation: Incocciati, A.; Bertuccini, L.; Boffi, A.; Macone, A.; Bonamore, A. Unlocking the Treasure Box: The Role of HEPES Buffer in Disassembling an Uncommon Ferritin Nanoparticle. *Separations* **2022**, *9*, 222. https://doi.org/10.3390/separations9080222

Academic Editor: Yu-Chie Chen

Received: 1 August 2022
Accepted: 14 August 2022
Published: 17 August 2022

1. Introduction

Nowadays, the use of nanoparticles as a drug delivery system (DDS) takes the forefront in cancer treatment [1–5]. The nanoparticles used are different in structure and composition, ranging from liposomes to more complex protein architectures [6–8]. Ferritins occupy a special place among protein nanoparticles due to their size, biocompatibility, and ability to recognize specific receptors on the cell surface [9,10]. Due to these features, ferritins have been extensively studied as nanovectors to deliver therapeutic and contrast agents [11–14]. From the structural point of view, ferritins consist of 24 subunits that associate to form a hollow sphere with an internal diameter of 8 nm (24-mer), capable of hosting molecules of different nature with adequate dimensions [15,16]. However, the ferritin must be dissociated and then reassociated in the presence of the selected cargo to perform this function. This step is the most critical of the whole process. Typically, the dissociation occurs at extreme pH values, which always leads to loss of protein and, at times, of the cargo itself [17–20]. This issue prompted researchers to investigate the structural determinants responsible for the nanoparticle self-assembly and design mutants that could dissociate under milder conditions [21,22].

The discovery of an uncommon ferritin in the thermophilic bacterium *A. fulgidus* (AfFt) boosted the research in this field [23]. AfFt is particularly promising for delivery purposes having an association/dissociation equilibrium mediated exclusively by the

saline concentration of the medium [24]. To make it suitable for recognizing the human transferrin receptor (TfR1), this was engineered by replacing its BC loop with the human H ferritin one [25,26]. The engineered protein named humanized *Archaeoglobus* ferritin (HumFt) is efficiently uptaken by cells and can carry different cargoes, including proteins and small therapeutic RNAs [27,28].

Unlike the human H ferritin, the quaternary structure of HumFt has four triangular pores about 4 nm wide, which could cause uncontrolled leakage when encapsulating small molecules. Previous studies have shown that two single amino acid substitutions (K150A and R151A) on AfFt result in a canonical quaternary structure, devoid of the triangular pores [29,30].

In this work, we introduced the same substitutions in HumFt and evaluated through chromatographic techniques whether they alter the ability to dissociate in mild conditions typical of *Archaeoglobus* ferritin. As a proof of concept, we demonstrated that this mutation avoids uncontrolled leakage when encapsulating small molecules such as curcumin, making it a promising theranostic tool.

2. Materials and Methods

2.1. Mutagenesis

K150A/R151A double mutation was introduced on HumFt gene using Stratagene's QuikChange® site-directed mutagenesis kit (Merck, Darmstadt, Germany), following the manufacturer's instruction. pET22HumFt plasmid, containing the HumFt synthetic gene optimized for the expression in *Escherichia coli* cells, was used as a PCR template. The mutagenic oligonucleotide primers were: forward 5′-CTGATTGGTGAAGATGCAGCTGCACTG CTGTTTCTGG-3′ and reverse 5′-CCAGAAACAGCAGTGCAGCTGCATCTTCACCAATC AG-3′. The PCR product was treated with DpnI enzyme to digest the template plasmid and then transformed into DH5α competent cells. Once the introduced mutations were checked by DNA sequencing, the resulting pET22HumFtR150A/K151A plasmid was transformed into BL21DE3 competent cells for protein expression.

2.2. Protein Expression and Purification

LB medium (6 L) was inoculated with overgrown BL21(DE3) cells containing pET22HumFtR150A/K151A plasmid, and protein expression was induced at OD600 = 0.6 with 1 mM IPTG at 37 °C. After 16 h, the bacterial cells were harvested by centrifugation and treated as described by Palombarini et al. [31] with slight modification. Briefly, the bacterial paste was resuspended in 20 mM HEPES buffer containing 50 mM $MgCl_2$ in the presence of a protease Inhibitor Cocktail (Basel, Switzerland). After sonication, the soluble fraction was subjected to two $(NH_4)_2SO_4$ precipitations (20% and 70%). The pellet from 70% $(NH_4)_2SO_4$ was recovered by centrifugation and extensively dialyzed versus 10 mM sodium phosphate buffer pH 7.2 containing 20 mM $MgCl_2$. The sample was digested with deoxyribonuclease I from bovine pancreas (Merck, Darmstadt, Germany), and DNA removal was achieved in a single step by means of crossflow ultrafiltration using a single Vivaflow 200 module (Sartorius) with a cutoff of 100 kDa, coupled to a Masterflex L/S pump system. Crossflow ultrafiltration was also used in diafiltration mode to exchange the buffer with 20 mM HEPES pH 7.4 containing 50 mM $MgCl_2$. Protein purity was monitored by SDS-PAGE (Biorad, Hercules, CA, USA). DNA removal was followed by measuring a 260/280 nm ratio using a Jasco V-650 spectrophotometer (JASCO Deutschland).

2.3. Chromatographic Analyses

Protein association/dissociation equilibrium was studied with different chromatographic techniques.

HP-SEC was performed using an Agilent Infinity 1260 HPLC apparatus (Agilent, Santa Clara, CA, USA) equipped with a UV detector. Separation was carried out using an Agilent AdvanceBio SEC 300 Å, 7.8 × 150 mm, 2.7 µm, LC column. Protein association/dissociation was evaluated by changing the mobile phase composition in the range of 20–150 mM HEPES

buffer pH 7.4 with or without $MgCl_2$. The separation was performed in isocratic mode at a flow rate of 0.7 mL/min. HumFtR150A/K151A elution was performed using UV detection at 280 nm. Protein standards were prepared in the same solution as the mobile phase.

Gel filtration analysis was performed using ÄKTA-Pure chromatography system (GE Healthcare) equipped with two different gel filtration columns (HiPrep™ 16/60 Sephacryl® S-300 HR (Cytiva, Danaher, Washington, DC, USA) and SepFastTM 16/60 6-600 HR (Clini-Science, Guidonia Montecelio, Italy)) with absorbance at 280 nm. Separation was carried at a flow rate of 0.6 mL/min using the following buffers as a mobile phase: (i) 20 mM HEPES pH 7.4, (ii) 150 mM HEPES pH 7.4, and (iii) 20 mM HEPES pH 7.4 containing 50 mM $MgCl_2$.

2.4. Transmission Electron Microscopy Negative Staining

Formvar-carbon coated grids were floated onto 30 µL of protein solutions (0.05–0.005 mg/mL) for adsorption (3 min). The excess of solution was blotted gently by filter paper, and the grids were air-dried and further stained with an aqueous solution of 1% (*w*/*v*) uranyl acetate for 3 min. The excess staining solution was removed carefully, and the grids were analyzed by an EM208S TEM (FEI—Thermo Fisher Scientific; Eindhoven—The Netherlands) at an acceleration voltage of 100 kV. Electron micrographs were taken with a slow scan camera (MEGAVIEW II, OLYMPUS).

High-magnification protein images were analyzed by the freeware software ImageJ (version 1.29, NIH, Bethesda, Rockville, MD, USA). Polymerized ferritins were approximated to an ellipse, and manual measurements of the areas with more than 100 particles were taken for each sample. The ferritin average diameters distribution was further calculated by Excel 2016.

2.5. Curcumin-Loaded Nanoparticles

An amount of 0.3 mL of a curcumin solution (30 mg/mL DMSO) was added to 10 mL of HumFtR150A/K151A and HumFt nanoparticles (10 mg/mL), dissociated in dimers in the presence of 150 mM and 20 mM HEPES buffer pH 7.4 respectively. Each ferritin sample was incubated in the dark under gentle stirring and then dialyzed versus 20 mM HEPES buffer containing 50 mM $MgCl_2$ for 48 h in the dark at room temperature. The incorporation of curcumin was evaluated through UV-vis absorption by measuring a 280/425 nm ratio (curcumin ε_{425} = 23,800 $M^{-1}cm^{-1}$).

3. Results and Discussion

Of all known ferritins, *Archaeoglobus*' ferritin (AfFt) has the unique feature of associating and dissociating by just varying the concentration of divalent cations: Mg^{2+} promotes the complete assembly of the 24-subunit sphere, which quickly dissociates into dimers when removing these ions. Furthermore, it has been shown that its quaternary geometry can change by replacing two basic amino acids with two aliphatic ones (K150A/R151A). These mutations lead to the conversion of the tetrahedral structure into the octahedral one, resulting in the closure of the large triangular pores typical of AfFt [29]. In this work, the same amino acid substitutions were introduced on the humanized ferritin of *A. fulgidus* (HumFt) to create a closed, easily dissociable nanoparticle that can recognize the TfR1 receptor (Figure 1).

DNA sequencing proved the correct replacement of the amino acids at positions 150 and 151 with two alanine residues. The resulting ferritin (HumFt K150A/R151A) is highly expressed in soluble form in *E. coli* and can be purified through a chromatography-free protocol, which involves fractional precipitations, thermal steps, filtrations, and ultrafiltration. At the end of the sequence, the protein is highly purified and free of contaminating DNA. UV absorption spectra (Figure 2) show that DNA removal, typically challenging for these proteins, is achieved after the last crossflow ultrafiltration step. Once purified, the ferritin was characterized by high-performance size-exclusion chromatography (HP-SEC) and transmission electron microscopy (TEM).

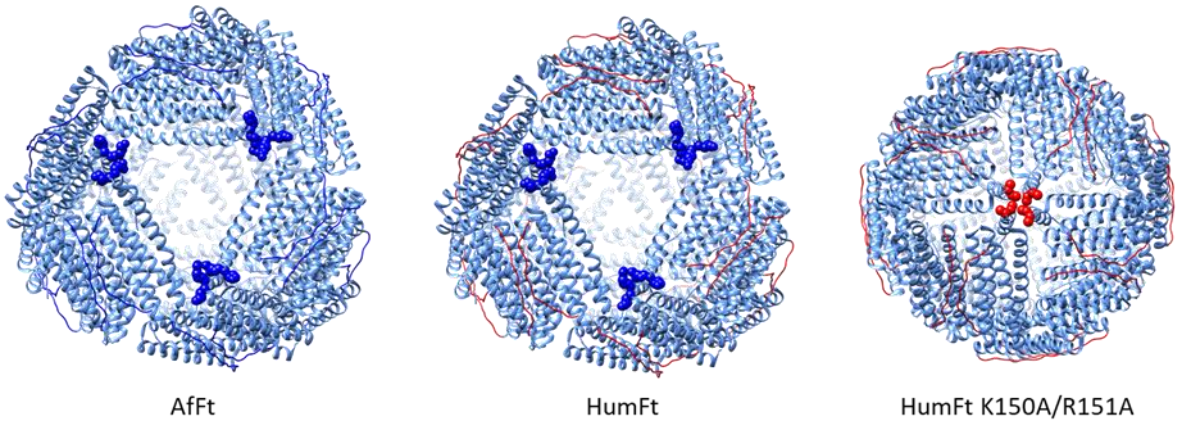

Figure 1. Structure of *A. fulgidus* ferritin (AfFt, pdb code 1S3Q), humanized *A. fulgidus* ferritin (HumFt, pdb code 5LS9) and humanized *A. fulgidus* ferritin double mutant (HumFt K150A/R151A, homology-modeling based on pdb codes 3KX9 and 5LS9). HumFt was obtained by grafting on AfFt the human H ferritin's BC loops (red loops). HumFt K150A/R151A derives from HumAfFt replacing K150 and R151 (highlighted in blue) with two alanine residues (highlighted in red). This double substitution results in the closure of the triangular pores.

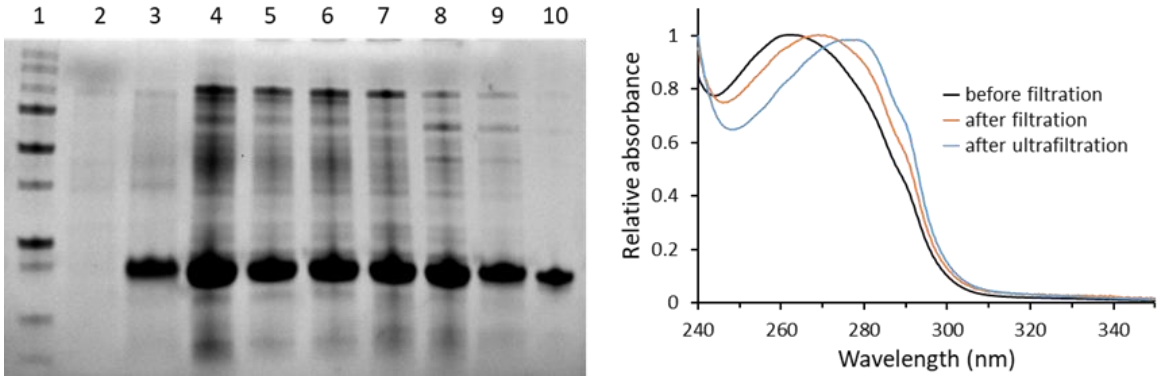

Figure 2. Protein expression and purification analyzed by SDS-PAGE and UV absorption. Lanes: 1. marker; 2. pre-induction; 3. post-induction; 4. sonication supernatant; 5. 20% ammonium sulfate supernatant; 6. 70% ammonium sulfate pellet; 7. soluble fraction after heat treatment at 62 °C; 8. soluble fraction after heat treatment at 72 °C; 9. sample filtered through diatomaceous earth; 10. sample filtered through Vivaflow200 module. DNA removal of samples 8, 9 and 10 was followed by UV absorption.

The amino acid substitutions introduced do not substantially alter the molecular weight of HumFt but should modify the overall geometry of the 24-mer, as occurs in AfFt [29]. The HP-SEC analysis (Figure 3) confirms that the mutant we produced is pure and correctly assembled according to the elution volume. Interestingly, unlike the protein from which it is derived, HumFtR150A/K151A has an association/dissociation equilibrium all shifted towards the closed 24-meric structure. This is the first important difference compared to HumFt, which, in the same experimental conditions, always keeps a percentage of dimer > 15% (Figure 3). The second difference is a shift in the elution volume of the 24-mer: HumFtK150A/K151A, having a lower molecular weight and a more compact geometry, elutes with a slight delay compared to HumFt.

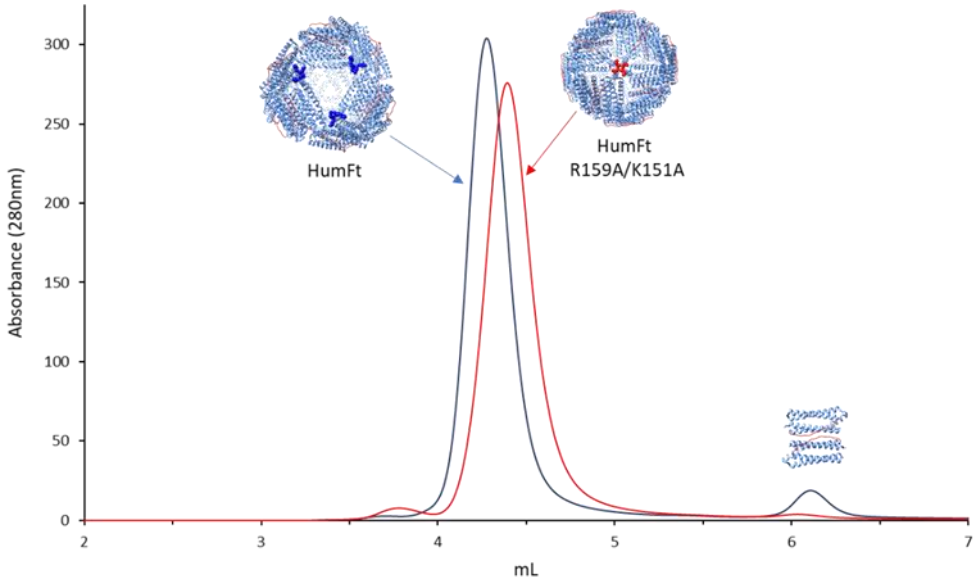

Figure 3. HP-SEC analysis of purified HumFt R150A/K151A compared to HumFt. When using 20 mM HEPES and 50 mm MgCl2 as the stationary phase, HumFt R150A/K151A is completely assembled (red chromatogram), whereas HumFt is partially dissociated as a dimer (blue chromatogram, 6.1 mL elution volume).

TEM imaging shows that HumFt R150A/K151A has the classic donut morphology of ferritins in which uranyl salt staining highlights the protein core (Figure 4). This represents direct evidence of the correct assembly of ferritin that is smaller than HumFt in diameter (11.58 nm versus 13.19 nm) [27], as confirmed by the chromatographic data.

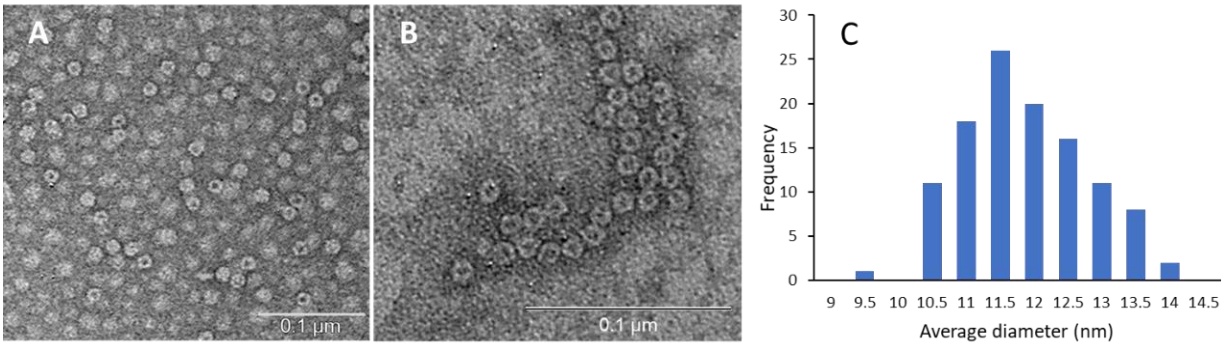

Figure 4. TEM imaging of HumFt R150A/K151A. TEM analysis was performed at different protein dilutions (panel (**A**) 0.5 µg/mL; panel (**B**) 0.005 µg/mL) in the presence of 20 mM HEPES buffer and 50 mM $MgCl_2$ (scale bar: 0.1 µm). Ferritin nanoparticles show the typical donut morphology with a diameter of 11.58 nm ± 0.9 (panel (**C**)).

This new ferritin can be suitable as a drug delivery system as long as it can be opened and closed without affecting the stability of both protein and cargo. Given that HumFt dissociates by removing magnesium ions from the medium, it is reasonable to assume that HumFtR150A/K151A also keeps the same features. We tested this hypothesis through HP-SEC. As expected, the 50 mM $MgCl_2$ and the 20 mM HEPES buffer solutions mediate the full assembly of the protein cage (Figure 3), but magnesium ion removal fails to promote efficient disassembly (Figure 5, blue chromatogram). Surprisingly, this behavior was not reported when the same amino acid substitutions were introduced on AfFt [29]. Indeed, the octahedral, closed structure of *Archaeoglobus* ferritin is 85% dissociated as a dimer in 25 mM HEPES buffer, without salt. Perhaps the simultaneous presence of both the double amino acid substitution and the human BC loop stabilizes this new ferritin in the 24-meric

form. The chromatographic conditions used (20 mM HEPES as mobile phase) lead to a poor peak resolution that does not allow an accurate evaluation of the protein shell disassembly. To improve resolution in the absence of magnesium ions, we tested mobile phases with increasing concentrations of HEPES. As shown in Figure 5, this strategy led to three outcomes: (i) as the buffer concentration increases, the 24-mer and dimer peaks are well resolved; (ii) HEPES by itself can favor the dissociation of 24-mer into dimer; and (iii) the maximum dissociation is obtained with 150 mM HEPES. At higher HEPES concentrations ($\geq$200 mM), about 20% of protein is lost without substantial improvement of the degree of dissociation.

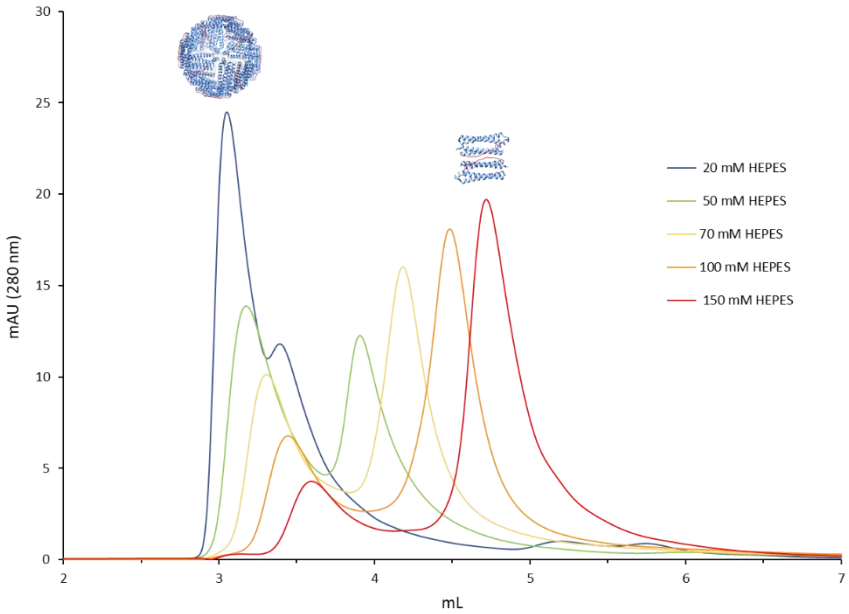

Figure 5. Effect of HEPES buffer concentration on HP-SEC analysis of purified HumFt R150A/K151A. Increasing HEPES buffer concentration from 20 mM to 150 mM leads to a better resolution of 24-mer and dimer, shifting at the same time the equilibrium towards the dimeric form.

To confirm that the concentration of the HEPES buffer could indeed favor the dissociation of the protein cage, we performed new experiments by changing the stationary phase. Specifically, we used two additional size-exclusion resins made of highly cross-linked polysaccharide composites of dextran and agarose (SepFast), or allyl dextran and N,N′-methylenebisacrylamide (Sephacryl). When the chromatographic separations were carried out on these columns, very similar results were obtained (Figure 6). Ferritin is fully assembled when the analysis is performed using 50 mM $MgCl_2$ and 20 mM HEPES as the mobile phase, while in the absence of magnesium ions (20 mM HEPES), it continues to be predominantly assembled (74.85 $\pm$ 13.8%). At 150 mM HEPES, the protein is mainly dissociated (85.3 $\pm$ 5.68% dimer, see Figure 6).

Our data show that HumFtR150A/K151A can be opened under mild conditions by simply changing the ionic strength of the buffer. Once disassembled, this ferritin must close just as easily to function as a drug delivery system. We show that adding $MgCl_2$ to a solution containing the opened ferritin (HEPES 150 mM) leads to the progressive and complete closure of the protein cage (Figure 7). Unlike HumFt, which never fully associates with high concentrations of $MgCl_2$, this mutant is already 100% associated with 30 mM $MgCl_2$.

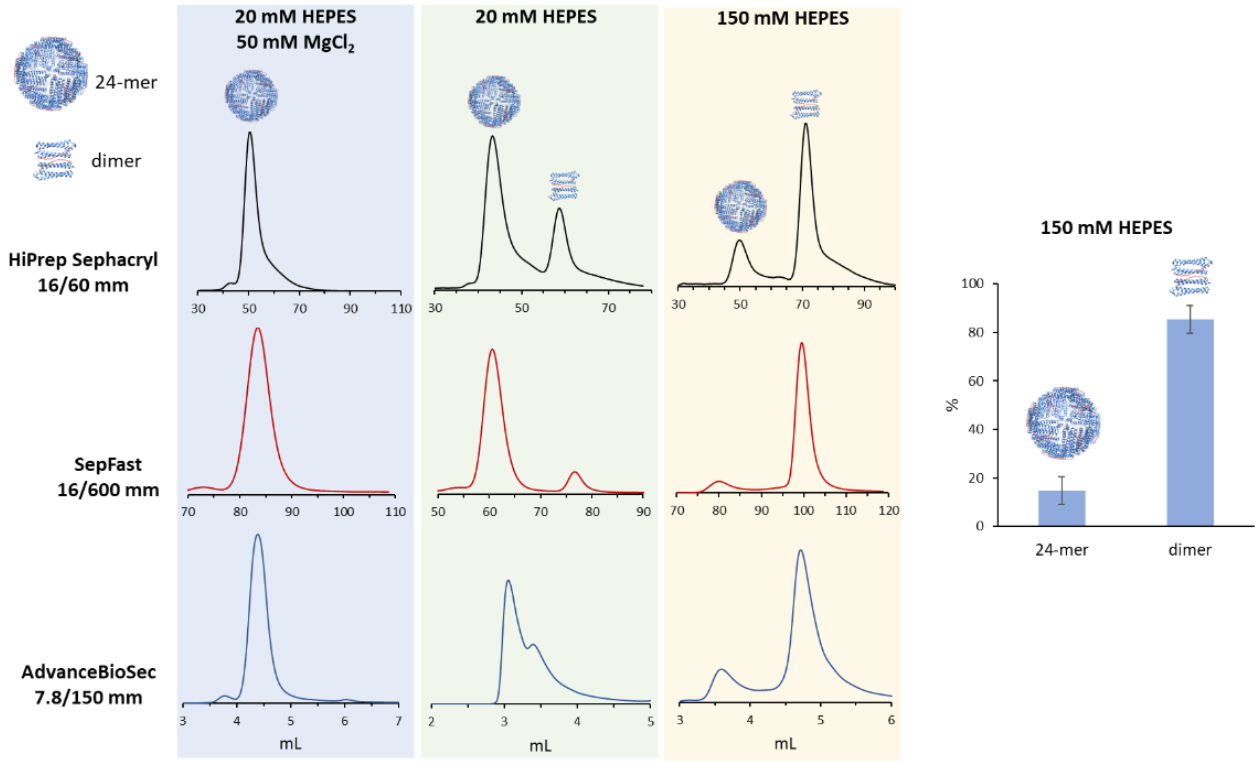

Figure 6. Size-exclusion chromatography of HumFtR150A/K151A. SEC analysis performed with three different stationary phases (HiPrep Sephacryl, SepFast and AdvanceBioSec) using different mobile phase compositions (20 mM HEPES containing 50 mM $MgCl_2$; 20 mM HEPES; 150 mM HEPES). At 150 mM HEPES, HumFtR150A/K151A is mainly present as a dimer (histogram on the right, data are presented as mean ± SD, n = 3).

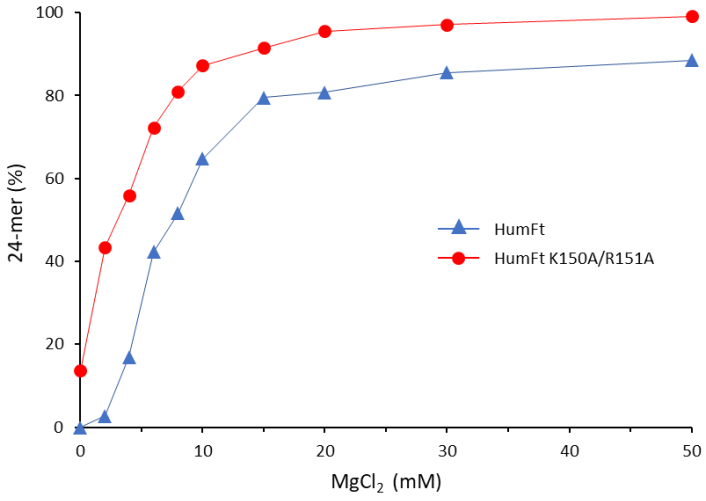

Figure 7. $MgCl_2$ effect on HumFtR150A/K151A assembly compared to HumFt. HumFtR150A/K151A in 150 mM HEPES buffer is dissociated at 15%. The addition of 50 mM $MgCl_2$ induces the complete closure of the protein cage (red line). At the same concentration of $MgCl_2$, HumFt is still partially dissociated (blue line).

The influence of buffer molecules on protein–protein interaction is a phenomenon recently studied in detail for many proteins. It was reported that the propensity of different ions to influence the aggregation state of proteins can be correlated to their hydration properties [32,33]. HEPES buffer, thanks to its positive viscosity index (0.60 at 25 °C and

pH 7.0), acts as a kosmotropic agent. It can interact with the positively charged amino acids on HumFtR150A/K151A surface, reducing the charge on the protein molecules, thus decreasing the electrostatic stabilization of the 24-mer. Conversely, the main effect of increasing $MgCl_2$ concentration might be the neutralization of the negatively charged amino acids by ion binding, thus lowering the electrostatic barrier to assembly.

As a proof of concept, to prove that the double mutation avoids the release of a given payload from the nanoparticle, we loaded both HumFt and HumFtR150A/K151A with curcumin. We selected curcumin because it is a small hydrophobic molecule with potential therapeutic applications and a characteristic absorption spectrum in the visible. When curcumin is encapsulated inside the protein cage, the visible spectrum shows a characteristic blue shift at 400 nm [34], which allows a rough estimate of the number of loaded molecules. By UV-vis spectrum analysis (Figure 8), about eighteen curcumin molecules are encapsulated within the HumFtR150A/K151A protein cage. When the loaded nanoparticle is dialyzed versus 20 mM HEPES buffer containing 50 mM $MgCl_2$, no uncontrolled leakage occurs over 48 hours (Figure 8). Under these experimental conditions, the 280/400 nm ratio is 0.7 for HumFtR150A/K151A, while it is considerably lower for HumFt (0.4).

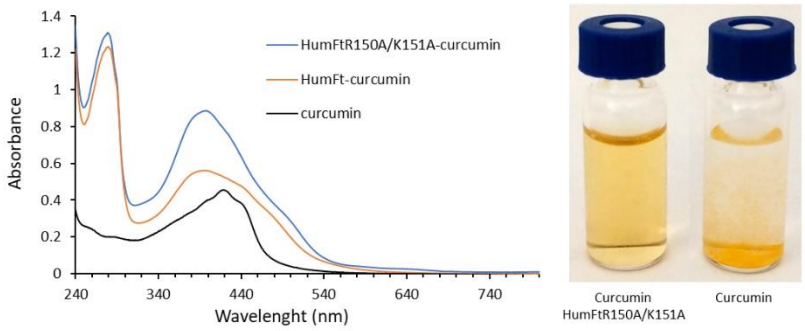

Figure 8. Loading of HumFtR150A/K151A and HumFt with curcumin. Left panel: UV-vis spectra of curcumin in 20 mM HEPES buffer pH 7.4 containing 50 mM $MgCl_2$ (black line) and of curcumin encapsulated in HumFtR150A/K151A (blue line) and in HumFt (orange line) after 48 hours dialysis. Right panel: Picture of samples containing HumFtR150A/K151A loaded with curcumin or curcumin alone in buffer.

4. Conclusions

In this paper, we have developed and characterized a new ferritin, which has high potential as DDS. This molecule derives from the humanized ferritin of *A. fulgidus*, on which two alanine residues have replaced two basic amino acids. These substitutions changed the overall geometry of the particle, closing the large triangular pores on its surface. In this way, it becomes suitable to encapsulate even small hydrophobic molecules such as curcumin, without leakage. We have shown that the assembly/disassembly of this new protein cage can be easily fine-tuned by varying the HEPES buffer and $MgCl_2$ concentration. In fact, the protein cage can be disassembled in 150 mM HEPES buffer in the absence of magnesium ions. When this divalent cation is added to the solution, the ferritin can reassemble as a 24-mer. The development of this new protein cage paves the way for encapsulation and delivery studies of small molecules for therapeutic and diagnostic purposes.

Author Contributions: Conceptualization, A.I., A.B. (Alessandra Bonamore) and A.M.; methodology, A.I. and L.B.; formal analysis, A.I. and L.B.; investigation, A.I. and L.B.; data curation, A.I.; writing—original draft preparation, A.B. (Alessandra Bonamore) and A.M.; writing—review and editing, A.B. (Alessandra Bonamore), A.M. and A.B. (Alberto Boffi); visualization, A.I.; supervision, A.B. (Alessandra Bonamore) and A.M.; project administration, A.B. (Alessandra Bonamore) and A.M.; funding acquisition, A.B. (Alberto Boffi). All authors have read and agreed to the published version of the manuscript.

Funding: This research received no external funding.

Institutional Review Board Statement: Not applicable.

Informed Consent Statement: Not applicable.

Data Availability Statement: All data related to the manuscript are available in the manuscript and in the form graphs, figures, and tables.

Conflicts of Interest: The authors declare no conflict of interest.

References

1. Yao, Y.; Zhou, Y.; Liu, L.; Xu, Y.; Chen, Q.; Wang, Y.; Wu, S.; Deng, Y.; Zhang, J.; Shao, A. Nanoparticle-Based Drug Delivery in Cancer Therapy and Its Role in Overcoming Drug Resistance. *Front. Mol. Biosci.* **2020**, *7*, 193. [CrossRef] [PubMed]
2. Van der Meel, R.; Sulheim, E.; Shi, Y.; Kiessling, F.; Mulder, W.J.M.; Lammers, T. Smart Cancer Nanomedicine. *Nat. Nanotechnol.* **2019**, *14*, 1007–1017. [CrossRef]
3. Noireaux, J.; Grall, R.; Hullo, M.; Chevillard, S.; Oster, C.; Brun, E.; Sicard-Roselli, C.; Loeschner, K.; Fisicaro, P. Gold Nanoparticle Uptake in Tumor Cells: Quantification and Size Distribution by Sp-ICPMS. *Separations* **2019**, *6*, 3. [CrossRef]
4. Niculescu, A.-G.; Grumezescu, A.M. Novel Tumor-Targeting Nanoparticles for Cancer Treatment—A Review. *Int. J. Mol. Sci.* **2022**, *23*, 5253. [CrossRef] [PubMed]
5. Iranpour, S.; Bahrami, A.R.; Nekooei, S.; Saljooghi, A.S.; Matin, M.M. Improving Anti-Cancer Drug Delivery Performance of Magnetic Mesoporous Silica Nanocarriers for More Efficient Colorectal Cancer Therapy. *J. Nanobiotechnol.* **2021**, *19*, 314. [CrossRef] [PubMed]
6. Kim, J.-S. Liposomal Drug Delivery System. *J. Pharm. Investig.* **2016**, *46*, 387–392. [CrossRef]
7. Kianfar, E. Protein Nanoparticles in Drug Delivery: Animal Protein, Plant Proteins and Protein Cages, Albumin Nanoparticles. *J. Nanobiotechnol.* **2021**, *19*, 159. [CrossRef]
8. Patra, J.K.; Das, G.; Fraceto, L.F.; Campos, E.V.R.; del Pilar Rodriguez-Torres, M.; Acosta-Torres, L.S.; Diaz-Torres, L.A.; Grillo, R.; Swamy, M.K.; Sharma, S.; et al. Nano Based Drug Delivery Systems: Recent Developments and Future Prospects. *J. Nanobiotechnol.* **2018**, *16*, 71. [CrossRef]
9. Montemiglio, L.C.; Testi, C.; Ceci, P.; Falvo, E.; Pitea, M.; Savino, C.; Arcovito, A.; Peruzzi, G.; Baiocco, P.; Mancia, F.; et al. Cryo-EM Structure of the Human Ferritin–Transferrin Receptor 1 Complex. *Nat. Commun.* **2019**, *10*, 1121. [CrossRef]
10. Wang, Z.; Gao, H.; Zhang, Y.; Liu, G.; Niu, G.; Chen, X. Functional Ferritin Nanoparticles for Biomedical Applications. *Front. Chem. Sci. Eng.* **2017**, *11*, 633–646. [CrossRef]
11. Khoshnejad, M.; Parhiz, H.; Shuvaev, V.V.; Dmochowski, I.J.; Muzykantov, V.R. Ferritin-Based Drug Delivery Systems: Hybrid Nanocarriers for Vascular Immunotargeting. *J. Control. Release* **2018**, *282*, 13–24. [CrossRef] [PubMed]
12. Mainini, F.; Bonizzi, A.; Sevieri, M.; Sitia, L.; Truffi, M.; Corsi, F.; Mazzucchelli, S. Protein-Based Nanoparticles for the Imaging and Treatment of Solid Tumors: The Case of Ferritin Nanocages, a Narrative Review. *Pharmaceutics* **2021**, *13*, 2000. [CrossRef] [PubMed]
13. Truffi, M.; Fiandra, L.; Sorrentino, L.; Monieri, M.; Corsi, F.; Mazzucchelli, S. Ferritin Nanocages: A Biological Platform for Drug Delivery, Imaging and Theranostics in Cancer. *Pharmacol. Res.* **2016**, *107*, 57–65. [CrossRef] [PubMed]
14. Calisti, L.; Trabuco, M.C.; Boffi, A.; Testi, C.; Montemiglio, L.C.; des Georges, A.; Benni, I.; Ilari, A.; Taciak, B.; Białasek, M.; et al. Engineered Ferritin for Lanthanide Binding. *PLoS ONE* **2018**, *13*, e0201859. [CrossRef]
15. Zhang, Y.; Orner, B.P. Self-Assembly in the Ferritin Nano-Cage Protein Superfamily. *Int. J. Mol. Sci.* **2011**, *12*, 5406–5421. [CrossRef]
16. Lawson, D.M.; Artymiuk, P.J.; Yewdall, S.J.; Smith, J.M.A.; Livingstone, J.C.; Treffry, A.; Luzzago, A.; Levi, S.; Arosio, P.; Cesareni, G.; et al. Solving the Structure of Human H Ferritin by Genetically Engineering Intermolecular Crystal Contacts. *Nature* **1991**, *349*, 541–544. [CrossRef]
17. Palombarini, F.; Di Fabio, E.; Boffi, A.; Macone, A.; Bonamore, A. Ferritin Nanocages for Protein Delivery to Tumor Cells. *Molecules* **2020**, *25*, 825. [CrossRef]
18. Kim, M.; Rho, Y.; Jin, K.S.; Ahn, B.; Jung, S.; Kim, H.; Ree, M. PH-Dependent Structures of Ferritin and Apoferritin in Solution: Disassembly and Reassembly. *Biomacromolecules* **2011**, *12*, 1629–1640. [CrossRef]
19. Stühn, L.; Auernhammer, J.; Dietz, C. PH-Depended Protein Shell Dis- and Reassembly of Ferritin Nanoparticles Revealed by Atomic Force Microscopy. *Sci. Rep.* **2019**, *9*, 17755. [CrossRef]
20. Mohanty, A.; K, M.; Jena, S.S.; Behera, R.K. Kinetics of Ferritin Self-Assembly by Laser Light Scattering: Impact of Subunit Concentration, PH, and Ionic Strength. *Biomacromolecules* **2021**, *22*, 1389–1398. [CrossRef]
21. Chen, H.; Zhang, S.; Xu, C.; Zhao, G. Engineering Protein Interfaces Yields Ferritin Disassembly and Reassembly under Benign Experimental Conditions. *Chem. Commun.* **2016**, *52*, 7402–7405. [CrossRef] [PubMed]
22. Calisti, L.; Benni, I.; Cardoso Trabuco, M.; Baiocco, P.; Ruzicka, B.; Boffi, A.; Falvo, E.; Malatesta, F.; Bonamore, A. Probing Bulky Ligand Entry in Engineered Archaeal Ferritins. *Biochim. Biophys. Acta BBA-Gen. Subj.* **2017**, *1861*, 450–456. [CrossRef] [PubMed]
23. Johnson, E.; Cascio, D.; Sawaya, M.R.; Gingery, M.; Schröder, I. Crystal Structures of a Tetrahedral Open Pore Ferritin from the Hyperthermophilic Archaeon Archaeoglobus Fulgidus. *Structure* **2005**, *13*, 637–648. [CrossRef] [PubMed]

24. Swift, J.; Butts, C.A.; Cheung-Lau, J.; Yerubandi, V.; Dmochowski, I.J. Efficient Self-Assembly of Archaeoglobus Fulgidus Ferritin around Metallic Cores. *Langmuir* **2009**, *25*, 5219–5225. [CrossRef]
25. De Turris, V.; Cardoso Trabuco, M.; Peruzzi, G.; Boffi, A.; Testi, C.; Vallone, B.; Celeste Montemiglio, L.; Georges, A.D.; Calisti, L.; Benni, I.; et al. Humanized Archaeal Ferritin as a Tool for Cell Targeted Delivery. *Nanoscale* **2017**, *9*, 647–655. [CrossRef]
26. Benni, I.; Trabuco, M.C.; Di Stasio, E.; Arcovito, A.; Boffi, A.; Malatesta, F.; Bonamore, A.; De Panfilis, S.; de Turris, V.; Baiocco, P. Excimer Based Fluorescent Pyrene–Ferritin Conjugate for Protein Oligomerization Studies and Imaging in Living Cells. *RSC Adv.* **2018**, *8*, 12815–12822. [CrossRef]
27. Palombarini, F.; Masciarelli, S.; Incocciati, A.; Liccardo, F.; Di Fabio, E.; Iazzetti, A.; Fabrizi, G.; Fazi, F.; Macone, A.; Bonamore, A.; et al. Self-Assembling Ferritin-Dendrimer Nanoparticles for Targeted Delivery of Nucleic Acids to Myeloid Leukemia Cells. *J. Nanobiotechnol.* **2021**, *19*, 172. [CrossRef]
28. Macone, A.; Masciarelli, S.; Palombarini, F.; Quaglio, D.; Boffi, A.; Trabuco, M.C.; Baiocco, P.; Fazi, F.; Bonamore, A. Ferritin Nanovehicle for Targeted Delivery of Cytochrome C to Cancer Cells. *Sci. Rep.* **2019**, *9*, 11749. [CrossRef]
29. Sana, B.; Johnson, E.; Le Magueres, P.; Criswell, A.; Cascio, D.; Lim, S. The Role of Nonconserved Residues of Archaeoglobus Fulgidus Ferritin on Its Unique Structure and Biophysical Properties. *J. Biol. Chem.* **2013**, *288*, 32663–32672. [CrossRef]
30. Sana, B.; Johnson, E.; Lim, S. The Unique Self-Assembly/Disassembly Property of Archaeoglobus Fulgidus Ferritin and Its Implications on Molecular Release from the Protein Cage. *Biochim. Biophys. Acta BBA-Gen. Subj.* **2015**, *1850*, 2544–2551. [CrossRef]
31. Palombarini, F.; Ghirga, F.; Boffi, A.; Macone, A.; Bonamore, A. Application of Crossflow Ultrafiltration for Scaling up the Purification of a Recombinant Ferritin. *Protein Expr. Purif.* **2019**, *163*, 105451. [CrossRef] [PubMed]
32. Brudar, S.; Hribar-Lee, B. Effect of Buffer on Protein Stability in Aqueous Solutions: A Simple Protein Aggregation Model. *J. Phys. Chem. B* **2021**, *125*, 2504–2512. [CrossRef] [PubMed]
33. Roberts, D.; Keeling, R.; Tracka, M.; van der Walle, C.F.; Uddin, S.; Warwicker, J.; Curtis, R. Specific Ion and Buffer Effects on Protein–Protein Interactions of a Monoclonal Antibody. *Mol. Pharm.* **2015**, *12*, 179–193. [CrossRef] [PubMed]
34. Chen, L.; Bai, G.; Yang, S.; Yang, R.; Zhao, G.; Xu, C.; Leung, W. Encapsulation of curcumin in recombinant human H-chain ferritin increases its water-solubility and stability. *Food Res. Int.* **2014**, *62*, 1147–1153. [CrossRef]